Single Particle Ignition and Combustion of Anthracite, Semi-Anthracite and Bituminous Coals in Air and Simulated Oxy-Fuel Conditions

Juan Riaza[1], Reza Khatami[2], Yiannis A. Levendis[2*], Lucía Álvarez[1], María V. Gil[1], Covadonga Pevida[1], Fernando Rubiera[1], José J. Pis[1]

[1] Instituto Nacional del Carbón, INCAR-CSIC, Apartado 73, 33080 Oviedo, Spain

[2] Mechanical and Industrial Engineering Department, Northeastern University, Boston, MA, 02115, USA

Abstract

A fundamental investigation has been conducted on the combustion behavior of single particles (75-150 μm) of four coals of different ranks: anthracite, semi-anthracite, medium-volatile bituminous and high-volatile bituminous. A laboratory-scale transparent laminar-flow drop-tube furnace was used to burn the coals, electrically-heated to 1400 K. The experiments were performed in different combustion atmospheres: air ($21\%O_2/79\%N_2$) and four simulated dry oxy-fuel conditions: $21\%O_2/79\%CO_2$, $30\%O_2/70\%CO_2$, $35\%O_2/65\%CO_2$ and $50\%O_2/50\%CO_2$. The ignition and combustion of single particles was observed by means of three-color pyrometry and high-speed high-resolution cinematography to obtain temperature-time histories and record combustion behavior. On the basis of the observations made with these techniques, a comprehensive examination of the ignition and combustion behavior of these fuels was achieved. Higher rank coals (anthracite and semi-anthracite) ignited heterogeneously on the particle surface, whereas the bituminous coal particles ignited homogeneously at the gas phase. Moreover, deduced ignition temperatures increased

---

[*] Corresponding author: Tel.: 001 (617) 373-3806; Fax: 001 (617) 373-2921
E-mail address: y.levendis@neu.edu

with increasing coal rank and decreased with increasing oxygen concentrations. Strikingly disparate combustion behaviors were observed depending on the coal rank. The combustion of bituminous coal particles took place in two phases. First, volatiles evolved, ignited and burned in luminous enveloping flames. Upon extinction of these flames, the char residues ignited and burned. In contrast, the higher rank coal particles ignited and burned heterogeneously. The replacement of the background N_2 gas of air with CO_2 (i.e., changing from air to an oxy-fuel atmosphere) at the same oxygen mole fraction impaired the intensity of combustion. It reduced the combustion temperatures and lengthened the burnout times of the particles. Increasing the oxygen mole fraction in CO_2 to 30-35% restored the intensity of combustion to that of air for all the coals studied. Volatile flame burnout times increased linearly with the volatile matter content in the coal in both air and all oxygen mole fractions in CO_2. On the other hand, char burnout times increased linearly or quadratically versus carbon content in the coal, depending on the oxygen mole fraction in the background gas.

1. Introduction

Coal has been, and will continue to be, one of the major energy resources in the long term because of its abundant reserves and competitively low price, especially for use in power generation. The share of coal in world energy consumption was 30.3% in 2011, as opposed to 33.1% for oil and 23.7% for natural gas [1]. A diverse power generation portfolio including Carbon Capture and Storage (CCS) technologies and renewable energies is needed to reduce atmospheric CO_2 to below 1990 levels [2]. The deployment

of oxy-fuel combustion in coal-fired utility boilers is seen as one of the major options for CO_2 capture. In this technology instead of using air as oxidizer, a mixture of oxygen and recycled flue gas (mainly CO_2 if dried) is employed to yield an effluent stream, rich in CO_2. However, the successful implementation of oxy-fuel combustion technology depends on fully understanding the difficulties that can arise from replacing nitrogen (inert) by CO_2 (reactive) in the oxidizer stream. Several factors such as char and volatile combustion or flame ignition and stability may be affected [3].

Previous work in this laboratory contrasted the combustion behaviors of single solid fuel particles of a bituminous high-volatile type-A coal, three low rank coals (low carbon content and low heating value coals): a sub-bituminous and two different lignites, as well as biomass (sugarcane bagasse) under air and under simulated dry oxy-firing conditions [4, 5]. This work aims at examining the combustion behavior of additional bituminous coals (high- and medium-volatile types-B) as well high rank coals (high carbon content and high heating value coals), i.e., anthracite and semi-anthracite. The combustion and emission studies of bituminous coals has been well-documented in the aforementioned studies of Khatami et al. and Kazanc et al. in this laboratory [4, 5, 6] as well as in other studies including those of [7-10]. However, studies on anthracite and semi-anthracite coal particle ignition and combustion are scarce.

There are several possible oxy-fuel combustion zones which are a function of the preheat temperature and oxygen mole fraction of the oxidant stream [11]. Air-like oxy-fuel combustion systems have been viewed not only as an appropriate technology for new units but also as a retrofit strategy for existing coal-fired power plants. Oxygen concentrations that are similar to, or higher than, those of air combustion systems are used in these oxy-fuel regimes (with a flue gas recycle rate of 60-80% vol, the oxygen

3

mole fraction is about 30% in the oxidizer stream) However, oxygen-enriched combustion (where the oxygen mole fraction is significantly higher than 21%) and full oxy-fuel combustion with neat oxygen are of industrial interest for several reasons (e.g., improved coal ignition, higher flame temperature, greater flame stability, reduction in boiler size and consequently lower plant costs).

The aim of the present work is to evaluate the effect of oxygen mole fraction on the ignition and combustion characteristics of bituminous and higher rank coals. The coals selected were burned in different O_2/CO_2 environments (21-50% O_2) in a laboratory-scale, electrically-heated, laminar-flow drop-tube furnace fitted with a transparent quartz tube. An air combustion atmosphere (i.e., $21\%O_2/79\%N_2$) was used as a baseline for comparison with O_2/CO_2 background gases. The ignition and combustion behavior of single particles was observed by means of three-color optical pyrometry and simultaneous high-speed high-resolution cinematography. The data obtained contributes to the understanding of coal combustion phenomena, in both air and in oxy-firing conditions.

2. Materials and methods

2.1. Coal samples

Four coals of different ranks were burned: an anthracite from Asturias, Spain (AC), a semi-anthracite from the Hullera Vasco Leonesa in León, Spain (HVN), a South African high-volatile bituminous coal supplied by the Aboño power plant in Asturias (SAB), and a medium-volatile bituminous coal from Mexico (UM). The semi-anthracite coal (HVN) is a physical blend of approximately 90% anthracitic and 10% low volatile bituminous coal from the same mine. The coals were ground and sieved to a particle

4

size cut of 75-150 μm. The fuels were dried prior to the experiments. Proximate analyses were obtained using a LECO TGA-601 in accordance with ASTM D7582-10 [12]. Ultimate analyses was determined using a LECO CHNS-932 instrument in accordance with ASTM D3176-89 [13]. Results of the analyses of the coals are presented in Table 1.

2.2. Experimental apparatus and procedure

The combustion studies of free-falling coal particles were performed in an electrically-heated laminar-flow drop-tube furnace, a detailed description of which has been provided elsewhere [14]. Here only a brief description of the reactor is given. The radiation cavity of the furnace (an *ATS* unit) is 25 cm long and is heated with molybdenum disilicide heating elements. A sealed transparent quartz tube with a 7-cm inner diameter was fitted in this furnace. A water-cooled injector was used to introduce single fuel particles at the top of the furnace (Fig. 1a). The furnace wall temperatures (T_f) were continuously monitored by means of type-S thermocouples embedded in the wall. The particle heating rates were high, calculated to be of the order of 10^4 K/s. Optical access to the radiation zone of the furnace was achieved through three observation ports: one at the top (used for pyrometry) and two orthogonally situated at the sides of the furnace (used for cinematography).

Pyrometric observations of the burning single particles were conducted from the top of the furnace injector, viewing downwards along the central axis of the furnace, as this ideally would be the particle's trajectory. In this way, complete luminous burnout histories of the single coal particles - from ignition to extinction - were recorded. Details of the pyrometer optics, electronics, calibration hardware and performance have been

reported elsewhere [15], so here only a brief description is provided. An optical fiber made up of a high-transmittance (> 99.5%) fused silica core and doped fused silica cladding with an f-number of 2.2, transmitted light from the furnace to the pyrometer assembly. The pyrometer used two dichroic edge filters as spectrum splitters to direct the light to the three interference filters (see Fig. 1b) having effective wavelengths of 0.640, 0.810 and 0.998 μm and bandwidths (FWHM) of 70 nm. In conjunction with the interference filters, silicon diode detectors were employed, the voltage outputs of which the represented spectral radiation intensities of burning particles. These signals were used to deduce particle temperatures [16].

High-speed cinematography was conducted through the slotted side quartz windows of the drop-tube furnace against backlight (Fig. 1a). A *NAC HotShot 512SC* self-contained digital high-speed video camera was used, set to speeds of 1000 or 2000 frames/s. The camera was fitted with an *Olympus-Infinity* Model K2 long-distance microscope lens to provide high-magnification images of the combustion events (see Fig. 1c).

The morphology of the coal chars was examined by means of scanning electron microscopy (SEM). Secondary electron images of the samples were obtained with a field emission scanning electron microscope (Quanta FEG-650-FEI) operated at 30 kV.

2.3. Furnace gas temperature and composition

Coal particle combustion experiments were conducted under quiescent gas conditions (i.e., no gas flow in the drop-tube furnace) in order to equalize the axial temperature profiles of N_2- and CO_2-containing furnace gases, as documented by Khatami et al. [5]. As shown in Fig. 2, under quiescent gas conditions (no flow), the axial gas temperature profiles in the furnace increased along its centerline and in a short distance from the

particle injector tip they reached asymptotically 1340 K. The gas compositions inside the furnace included air as well as the following four binary mixtures of O_2/CO_2 ($21\%O_2/79\%CO_2$, $30\%O_2/70\%CO_2$, $35\%O_2/65\%CO_2$ and $50\%O_2/50\%CO_2$).

3. Results

3.1 Temperature-time history of coal particles

Typical examples of radiation intensity-time and temperature-time profiles of single coal particles during their entire burnout history in air-firing conditions are displayed in Fig. 3. The radiation intensity traces were represented by the output voltage signals S_n of all three wavelength channels of the pyrometer. The temperature deduction method has been described in Ref. [16].

In the case of the bituminous coal two separate combustion phases were distinguished by three-color pyrometry (see Figs. 3c and 3d). In contrast, the anthracitic and most of the semi-anthracite coal particles experienced only one combustion phase (see Figs. 3a and 3b).

3.2 High-speed cinematography stills

Selected images from high-speed, high-resolution cinematography of particles of the four coals burning in air ($21\%O_2/79\%N_2$) and in three of the simulated oxy-fuel atmospheres studied ($21\%O_2/79\%CO_2$, $30\%O_2/70\%CO_2$ and $50\%O_2/50\%CO_2$), are shown in Figs. 4-7.

Most of the AC coal particles in air burned with no evidence volatile matter flames (see Fig. 4). These coal particles ignited and burned heterogeneously by direct attack of oxygen on their surfaces. Due to the known low reactivity of the anthracite AC particles

[17], their ignition was delayed. The color of the particles changed from dark (black) to bright (nearly-white) as their surfaces became incandescent; this change occurred gradually over a few milliseconds.

As the HVN coal is a physical blend of approx. 90% anthracitic and 10% low volatile bituminous coal from the same mine, most HVN coal particles burned in the same way as the AC anthracite coal particles. A few particles, however, experienced small enveloping flames attributed to combustion of volatiles (see Fig. 5, second frames in first and fourth cases). Once the flames were extinguished, the resulting chars proceeded to burn heterogeneously.

The two bituminous coals of this study, UM and SAB, experienced similar combustion trends, as exemplified in Figs. 6 and 7, including homogeneous ignition and combustion of volatiles in envelope flames, followed by heterogeneous ignition, combustion and extinction of the resulting chars. The volatiles produced large sooty flames that ignited in the gas phase and completely surrounded individual particles. The different relative velocities between the free-falling particles and surrounding furnace gas led to the formation of con-trails that burned in the wake of the particles; sometimes the gas flames expanded backwards from the particles. Since the volatiles contain tars, in some cases drops of burning tars can be distinguished inside the flame as sources of high luminosity. Tars need more time to burn up, hence occasionally some of these drops continued to burn while the flame burned out. In atmospheres containing 21% O_2 the drops were sometimes quenched before completely burning out resulting in the formation of soot ligaments. This phenomenon was especially noticeable in the $21\%O_2/79\%CO_2$ atmosphere. Upon extinction of a volatile flame, the luminous combustion of the char commenced. The recorded cinematographic images suggest the

final diameters of the chars approached those of the estimated size of ash residues, as discussed in the Appendix.

For the four coals studied, when N_2 was replaced with CO_2, keeping the oxygen mole fraction constant, the burning particles appeared dimmer. This is indicative of slower oxidation, which causes lower flame/particle temperatures. Dim combustion was also observed by Zhang et al. [18], who reported that the average intensity of coal particles burning in O_2/CO_2 with oxygen concentrations below 30%, was much lower than that in air. Moreover, in our study the brightness and intensity of combustion increased drastically with O_2 in the O_2/CO_2 environments, which is indicative of rapid oxidation. In fact, particle combustion images of the $30\%O_2/70\%CO_2$ atmosphere resembled those in air.

3.3 Morphology of coal chars

The chars obtained from coal devolatilization under N_2 and CO_2 background gases in an entrained reactor were examined by SEM; sample images are shown in Fig. 8. These photographs were obtained in prior experiments, described in Ref. [19], at an average reactor gas temperature of 1273 K. This temperature is in the range of gas temperatures encountered in the experiments herein in the region of the furnace herein where particle devolatilization has been observed to take place prior to ignition, i.e., in the first centimeter of the furnace, see temperature profile shown in Fig. 2. As shown in Fig. 8, the anthracite (AC) and the semi-anthracite (HVN) coal chars consist of angular solid particles with sharp edges. The AC chars have sharper edges (see Fig. 8a,b,e,f) than the HVN chars. The medium volatile bituminous UM chars have striking bubble-like network-type structures (Fig. 8c, g). The particles must have exhibited intense swelling

and bubbling during devolatilization to form cenospheric char particles with almost transparent walls. Large blow-holes often appear on the surfaces, particularly in CO_2 (Fig. 8g). Cenospheric char formation with associated swelling was also observed in the case of the high-volatile bituminous SAB particles (Figs. 8d, h). However, the walls of the SAB cenospheres appear to be much thicker and much more opaque than those of the UM cenospheres.

4. Discussion

The ignition and combustion behavior of anthracite, semianthracite and bituminous coal particles were determined based on the combined diagnostic techniques of pyrometry and back-light cinematography, in conjunction of scanning electron microscopy.

4.1. Ignition phenomena and ignition temperatures

(a) Ignition mode

Ignition-related events of anthracite, semi anthracite and bituminous coal particles, are illustrated in the initial stills of the photographic sequences depicted in Figs 4-7. The determination of ignition mode in this work relied on luminous emissions. Anthracite and semi-anthracite coal particles ignited heterogeneously on the particle surfaces. Such ignition mode is attributed to the low volatile matter content and high fixed carbon content of these coals. In the case of a few semi-anthracite particles, gas-phase (homogeneous) ignition took place due to their higher volatile matter content as discussed earlier. The nature of the heterogeneous ignition of anthracite and semi-anthracite particles is however different to that of lignite coals, previously studied in this laboratory [5]. Although the lignite coal particles contained sufficient amounts of

volatile matters for gas-phase ignition, their extensive fragmentation and the small fragment sizes were the main reasons for their heterogeneous ignition [5]. The much higher volatile content bituminous coal particles of this study ignited in the gas phase (homogeneously). The homogeneous ignition mode of bituminous coal in the current study is in line with previous observations in this laboratory for the Pittsburgh #8 high-volatile bituminous coal [5].

(b) Ignition Temperatures

In this study, ignition temperature was defined as the first point where the maximum particle temperature gradient (dT_p/dt) was recorded, see Fig. 9a. Fig. 9b shows the ignition temperatures in air as well as in different O_2/CO_2 atmospheres for various fuels, under the conditions of this study. Each data point in this figure represents average ignition temperatures from at least 8 randomly-selected particles. Ignition temperature data for lignite coal particles from a previous study in this laboratory [4] are also displayed in this figure for comparison.

Fig.9 illustrates that higher rank coals ignited at higher temperatures. Moreover, replacing N_2 with CO_2 increased the ignition temperature, but only negligibly. Increasing oxygen mole fraction in CO_2 consistently decreased the ignition temperature for all coal ranks.

4.2. Combustion mode

Single particle combustion modes were discussed comprehensively in previous studies [4, 5, 20]. In summary, Howard and Essenhigh [20] studied the combustion phenomena of coal particles and proposed a model to assess whether the burning of the volatiles and

char takes place sequentially or simultaneously. Khatami et al. [4, 5] employed that model to a number of coals from different ranks in a variety of oxygen-nitrogen and oxygen-carbon dioxide environments. The terms *two-mode* and *one-mode* combustion were used to respectively signify events where gas-phase combustion of the volatiles takes place in an enveloping flame, prior to heterogeneous char particle combustion, and where volatile and solid char combustion take place simultaneously.

(a) *Anthracitic* and the majority *of semi-Anthracite coal* particles exhibited only one wide peak in each pyrometric profile, which is attributed to heterogeneous combustion of the char (see Figs. 3a and 3b) with possible simultaneous burning of volatiles. This observation is consistent with the cinematographic behavior, where there is no evidence of an enveloping flame corresponding to volatiles combustion, but only that of the incandescent burning char. Such anthracitic coals produced no incandescent trails of volatiles (see Figs. 4 and 5). Moreover, most of the anthracite particles and some semi-anthracite particles exhibited striking undulation patterns (wave patterns) in their radiation intensity pyrometric signals. As the deduced temperature profiles do not show such undulations, but deduced luminous cross sectional areas do (with a method outlined in Ref. [16]), such conspicuous undulation patterns were attributed to particle rotations during combustion. Such patterns can indeed be detected in cinematographic sequences as the one shown in Fig.10. Somehow the anthracite char particles, which as documented earlier (see Section 3.3) retain their planar and angular shapes upon devolatilization and supposedly throughout char combustion, experienced rotation (tumbling) as they fell in the drop tube furnace. These coals are non swelling and they release much fewer volatiles than the bituminous coals, as also reported by Seeker at al. [21].

12

(b) The *bituminous coal* particles exhibited two peaks in each profile, an exceedingly strong first peak followed by a less pronounced second peak (see Figs. 3c and 3d). The first peak is attributed to volatiles burning homogeneously in luminous enveloping flames, whereas the second peak is attributed to the heterogeneous combustion of char. The combustion of the chars was lengthy and bright. The bituminous coals are rich in volatile hydrocarbons and tars, some of which are soot precursors [22]. Bituminous coals typically swell up and form cenospheric spheroid chars, as illustrated in section 3.3. In doing so, they expel volatiles in jets or trails (e.g. Fig. 6, 30%O_2/70%CO_2, 8 ms, Fig. 7, 21%O_2/79%N_2, 23 ms), forming condensed matter around a particle. In the regions where there are no jets of volatiles, there is a possibility of heterogeneous surface reaction with oxygen. The temperatures of most bituminous chars experienced small variations with time, whereas the radiation intensity and particle diameter plateaued for a time and then, slowly decreased. This behavior of the bituminous particles is clearly illustrated in the cinematographic images (see Figs. 6 and 7), and has been well documented in the literature [4, 14, 21, 23, 24].

4.3. Effect of fuel type on temperature and burnout time

The burnout time data and temperatures are shown in Figs. 11 and 12, respectively. The pyrometric burnout times are based on the duration of the pyrometer signal from its onset (particle ignition) to its termination (particle extinction), both defined herein when the highest-intensity signal ($\lambda = 998$ nm) of a particular event exceeds the baseline by a factor of at least ten, i.e., $S_{signal}/S_{baseline} > 10$. The temperatures displayed were the maximum temperatures deduced from the single particle combustion histories (as

exemplified in Fig. 3). Each data point represents the mean values from at least 15-20 individual particle combustion events.

In this sub-section only the examples in the air atmosphere are described for a clearer comparison between the coals. The burnout times of the bituminous particles were much shorter than the burnout times of the anthracitic particles. This may be due to the higher volatile matter content of the bituminous coals (which enhances subsequent char combustion), and to their higher reactivity. As high rank coals release few volatiles, there were very small differences between the chars and the original coal particles. On the other hand, in the case of the bituminous coals, their chars showed significant signs of swelling after devolatilization [19]. This created more specific surface area, and therefore enhanced particle reactivity. As can be seen from Fig. 11, the burnout times in air for the anthracitic coals were the longest, 294 ms and 215 ms for AC and HVN, respectively; whereas for bituminous coals UM and SAB the burnout times were 114 ms and 86 ms, respectively.

As can be seen in the cinematographic records, bituminous coals displayed a tendency to burn in *two-mode* combustion. Volatiles often contain a large amount of stored energy (heating value) and, as can be seen in Fig. 12, the combustion of volatiles was the hottest and the fastest (typically lasting 10-15 ms in air). Lower temperatures were reached during char combustion. The high-volatile bituminous SAB coal contained the highest amount of volatile matter. The average temperatures reached during its combustion in air were also the highest, 2079 K and 1795 K for volatiles and char, respectively, whereas in the combustion of the medium volatile bituminous UM coal in air, which has a lower volatile matter content, average temperatures of 1967 K and 1686 K were reached for volatiles and char, respectively. On the other hand, anthracitic coals

burned in *one-mode* combustion by direct attack of oxygen on the char surface. During the combustion of AC and HVN in air, the average char temperatures reached were 1825 K and 1811 K, respectively.

4.4. Effect of the diluent background gases (N_2 and CO_2) and oxygen mole fraction on temperatures and burnout times

As can be seen in Fig. 12 the particle temperatures (in the case of bituminous coals for both volatiles and chars) were higher during their combustion in $21\%O_2/79\%N_2$ than in $21\%O_2/79\%CO_2$, whereas their corresponding burnout times were shorter (see Fig. 11). A factor controlling the particle temperatures is the volumetric heat capacity of the surrounding gas mixture, which is higher in O_2/CO_2 than in O_2/N_2, atmospheres causing both the volatile mater flame temperatures and the char temperatures to drop [4, 8, 25]. Other important factors which influence char combustion temperature are the lower binary diffusion of O_2 in CO_2 and the endothermicity of the char-CO_2 reactions [25, 26, 27]. Larger CO concentrations, formed partly due to incomplete combustion of the volatiles, and partly driven from char CO_2 gasification reactions, would also contribute to the worsening of the burning properties of the coal, by forming a persistent cloud around the particle, thereby preventing the access of oxygen to the surface of the particle [17].

The particle temperature (in the case of the bituminous coals for both the char and the volatiles) increased and the burnout times decreased with the enhancement of the oxygen content in the CO_2 mixture. However, the shortening in the burnout times and the enhancement of temperatures was not the same for all the coals studied. It was more marked in the case of the anthracitic coals since the bituminous coals reached a high

burnout value in atmospheres with lower oxygen content (i.e., $21\%O_2/79\%N_2$ and $21\%O_2/79\%CO_2$) [28] . Increasing the O_2 percentage in the CO_2 mixture up to 50% was still insufficient to match the heat capacity of air (Heat capacity of pure gases (at 1400K) are N_2 34.18kJ/kmol-K; O_2 36.08 kJ/kmol-K and CO_2 57.83kJ/kmol-K. Therefore, heat capacity of the air and some of the O_2/CO_2 environments in this study are: Air=34.6 kJ/kmol-K, $21\%O_2/79\%CO_2$=53.3 kJ/kmol-K, $50\%O_2/50\%CO_2$= 47 kJ/kmol-K). However, the rise in the mass flux rate increased the reactivity characteristic of the local mixture [27]. Bejarano et al. [8] found that the higher the oxygen mole fraction, the higher the char surface temperature and the shorter the burnout time. In addition, if there is sufficient oxygen, the homogeneous combustion of the gasification-derived CO to CO_2 could provide extra heat. Joutsenoja et al. [29] measured temperature snapshots of burning single particles in an entrained flow reactor using a pyrometric method, when the oxygen mole fraction ranged between 3 and 30% and they also reported that the particle temperature increased with oxygen mole fraction.

In summary, coals burned hotter and faster in N_2 than in CO_2 background gases at comparable oxygen mole fractions. To attain the same volatiles flame and char temperatures as in air ($21\%O_2$), the oxygen content in CO_2 mixtures had to be increased to ~35% for these bituminous coals, and to ~30% for these anthracitic coals The values of oxygen needed to achieve the same particle char and volatiles temperatures in oxy-fuel conditions as in air-firing, are shown in Table 2. Increasing the oxygen concentration to such values also led to shortened burnout times and temperature hikes, although they are less remarkable. These results are in agreement with previous studies carried out for other fuels with different experimental devices [10, 30, 31]. These

observations have practical ramifications in the operation of future furnaces operating under oxy-coal combustion conditions. The successful implementation of O_2/CO_2 technology in conventional pulverized coal boilers requires a full understanding of the changes that occur when N_2 is replaced by CO_2 in a combustion atmosphere; this is essential for designing and modeling oxy-fuel combustion at an industrial scale. One should keep in mind however, that had combustion occurred in active flow conditions in the furnace and not under the quiescent conditions of this study (which resulted in the gas temperature profiles depicted in Fig.2) the O_2/CO_2 gas temperatures would have been lower than the O_2/N_2 gas temperatures, since CO_2 heats up slower [5]. This would have resulted in lower coal particle temperatures in CO_2 background gases than those reported herein. Hence, somewhat higher oxygen mole fractions in CO_2 would have been needed than those shown in Table 2 to match the particle temperatures in conventional air combustion. Alternatively, preheating of the O_2/CO_2 gases could have been implemented to compensate for their slower heating in the furnace. In this case the mole fractions listed in Table 2 may still be valid, depending on the degree of preheating.

4.5. Effect of volatile matter (VM) content on the volatile flame burnout times

Figure 13 shows the volatile flame burnout times of the different coals in this study versus volatile matter content of the fuels burning in air and in various O_2/CO_2 atmospheres. The volatile burnout times increased linearly with increasing volatile matter content (VM) of the coals in all gas environments. The linear dependency equations of volatile burnout times ($t_{volatiles}$) and volatile matter content in the coal (VM) are shown in Fig 13. It should be mentioned that the linear equations in Fig.13 were

17

derived for the experimental conditions of this study (i.e., T_f=1400 K and particle sizes 75-150µm) and may not be necessarily valid for different experimental/operating conditions.

4.6. Effect of carbon content (C) on the char burnout times

Figure 14 shows the char burnout times of different coals versus carbon content of the fuels burning in air and in various O_2/CO_2 atmospheres. The char burnout times increased with increasing carbon content (C) of the coals in all gas environments. However, the dependency of char burnout times versus carbon content (C) was quadratic for air and lower oxygen mole fractions in CO_2 (21%O_2), whereas this dependency became linear at higher O_2 mole fractions (35%O_2, 50%O_2). The quadratic and linear equations of char burnout times (t_{char}) versus carbon content of the coal (C) are also displayed in Fig. 14. It should be again mentioned that the equations shown in Fig. 14 were derived for the experimental conditions of this study (T_f=1400 K and particle sizes 75-150µm) and, again, may not be necessarily valid for different experimental/operating conditions.

5. Conclusions

Pulverized fuel particles (75-150 µm) from four high and medium rank coals were burned in a drop-tube furnace, set at 1400 K under air and simulated dry oxy-firing conditions. The goal was to assess the ignition and combustion behaviors of single coal particles in different combustion atmospheres with combined cinematographic and pyrometric diagnostic tools. The most important conclusions are as follows:

18

(a) High rank coals (anthracite and semi-anthracite) ignited heterogeneously from the particle surface, whereas bituminous coals ignited in the gas phase (homogeneously).

(b) Ignition temperatures increased with the enhancement of coal rank in either air or oxy-fuel combustion conditions. However, increasing oxygen mole fraction from 21% to 50% in CO_2 decreased the ignition temperature for all coals.

(c) Replacing the N_2 in air by CO_2 slightly increased the ignition temperature (30-40K).

(d) The two bituminous coal particles tested burned with distinct volatile matter and char combustion phases (i.e., two-mode combustion), whereas the anthracitic and most semi-anthracite coal particles burned in a single combustion phase, which was mostly attributed to char. The temperatures of the bituminous coal char particles were lower than those of the anthracitic coals, and their combustion durations were much shorter.

(e) For the four coals studied, particle luminosity and the deduced temperatures were higher in the $21\%O_2/79\%N_2$ atmosphere than in $21\%O_2/79\%CO_2$. The replacement of N_2 by CO_2 reduced the bituminous volatiles flame temperatures by as much as 210 K, and coal char surface temperatures by as much as 140 K, at comparable oxygen mole fractions. The corresponding drop for anthracitic coals was around 125 K. The combustion times increased by as much as 60 ms in the case of the anthracitic coals, and 30 ms in the case of bituminous coals.

(f) As the oxygen concentration in the CO_2 mixtures increased from 21% to 50%, the temperature of the char particles increased up to 320 K for the anthracitic coals and 310 K for the bituminous coals. The temperature of the volatiles

increased by as much as 400 K for the bituminous coals. Also an important reduction in burnout time was observed, especially in the case of anthracitic coals.

(g) Equivalent bituminous coal volatiles and char temperatures as well as burnout times to those measured in air were attained when the oxygen content in the CO_2 mixtures was ~30-35%. This observation has practical ramifications in the operation of practical systems.

(h) The volatile burnout times increased linearly with increasing volatile matter content (VM) of the coals in all gas environments.

(i) The dependency of char burnout times versus carbon content (C) was quadratic for air and lower oxygen mole fractions in CO_2 (21%O_2) while this dependency was linear at higher O_2 mole fractions (35%O_2, 50%O_2).

Acknowledgment

References
1. BP, Statistical Review of World Energy, 2012.
2. IEA, World Energy Outlook, 2011.
3. M.B. Toftegaard, J. Brix, P.A. Jensen, P. Glarborg, A.D. Jensen, Progr. Energy Combust. Sci. 36 (2010) 581-625.
4. R. Khatami, C. Stivers, K. Joshi, Y.A. Levendis, A.F. Sarofim, Combust. Flame 159 (2012) 1253-1271.
5. R. Khatami, C. Stivers, Y.A. Levendis, Combust. Flame 159 (2012) 3554-3568.

6. F. Kazanc, R. Khatami, P.M. Crnkovic, Y.A. Levendis, Energy Fuels 25 (2011) 2850-2861.
7. J. Faúndez, B. Arias, F. Rubiera, A. Arenillas, X. García, A.L. Gordon, J.J. Pis, Fuel 86 (2007) 2076-2080.
8. P.A. Bejarano, Y.A. Levendis, Combust. Flame 153 (2008) 270-287.
9. L. Zhang, E. Binner, Y. Qiao, C.-Z. Li, Fuel 89 (2010) 2703-2712.
10. Y. Liu, M. Geier, A. Molina, C.R. Shaddix, Int. J. Greenhouse Gas Control S5 (2011) S36-S46
11. L. Chen, S.Z. Yong, A.F. Ghoniem, Prog. Energy Combust. Sci. 38 (2012) 156-214.
12. ASTM, ASTM D7582: Standard Test Methods for Proximate Analysis of Coal and Coke by Macro Thermogravimetric Analysis. Annual Book of ASTM Standards. American Society for Testing and Materials, West Conshohocken, PA, 2010.
13. ASTM, ASTM D3176-89: Standard practice for ultimate analysis of coal and coke. Annual Book of ASTM Standards. American Society for Testing and Materials. West Conshohocken, PA, 2002.
14. Y.A. Levendis, K. Joshi, R. Khatami, A.F. Sarofim, Combust. Flame 158 (2011) 452-465.
15. Y.A. Levendis, K.R. Estrada, H.C. Hotel, Review Sci. Instruments 63 (1992) 3608-3622.
16. R. Khatami, Y.A. Levendis, Combust. Flame 158 (2011) 1822-1836.
17. M.V. Gil, J. Riaza, L. Álvarez, C. Pevida, J.J. Pis, F. Rubiera, Energy 48 (2012) 510-518.
18. L. Zhang, E. Binner, L. Chen, Y. Qiao, C.-Z. Li, S. Bhattacharya, Y. Ninomiya, Energy Fuels 24 (2010) 4803-4811.
19. M.V. Gil, J. Riaza, L. Álvarez, C. Pevida, J.J. Pis, F. Rubiera, Appl. Energy 91 (2012) 67-74.
20. J.B. Howard, R.H. Essenhigh, Proc. Combust. Inst. 11 (1967) 399-408.
21. W.R. Seeker, G.S. Samuelsen, M.P. Heat, J.D. Trolinger, Proc. Combust. Inst. 18 (1981) 1213-1226.
22. A. Ergut, S. Granata, J. Jordan, J. Carlson, J.B. Howard, H. Ritcher, Y.A. Levendis, Combust. Flame 144 (2006) 757-772.
23. L.D. Timothy, A.F. Sarofim, J.M. Beer, Proc. Combust. Inst. 19 (1982) 1123-1130.
24. W.J. McLean, D.R. Hardesty, J.H. Pohl, Proc. Combust. Inst. 18 (1981) 1239-1248.
25. T. Maffei, R. Khatami, S. Pierucci, T. Fravelli, E. Ranzi, Y.A. Levendis, Combust. Flame (2013), http://dx.doi.org/10.1016/jcombustflame.2013.06.002
26. C.R. Shaddix, A. Molina, Proc. Combust. Inst. 32 (2009) 2091-2098.
27. A. Molina, C.R. Shaddix, Proc. Combust. Inst. 31 (2007) 1905-1912.
28. J. Riaza, L. Álvarez, M.V. Gil, C. Pevida, J.J. Pis, F. Rubiera, Energy 36 (2011) 5314-5319.
29. T. Joutsenoja, J. Saastamoinen, Energy Fuels 13 (1999) 130-145.
30. J. Riaza, M.V. Gil, L. Álvarez, C. Pevida, J.J. Pis, F. Rubiera, Energy 41 (2012) 429-435.
31. Q. Li, C. Zhao, X. Chen, W. Wu, B. Lin, Chem. Eng. Process. Intensif. 49 (2010) 160-164.
32. Y.A. Levendis, R.C. Flagan, G.R. Gavalas, Combust. Flame 76 (1989) 221-241.
33. J.E. Metcalfe, M. Kawahata, P.L. Walker, Molecular Sieve Properties of Activated Anthracite. Fuel Technology Department report, Penn state University, 41-46.

Appendix

Calculation of diffusion-limited burnout times

The average oxygen mole fraction on the char particle surface can be estimated by the following formula [32]:

$$y_{O_2s} = (4/3 + y_{O_2\infty})\,\mathrm{e}^{-(\frac{a_0^2 R T_m \rho_c}{56 P_{tot} D t_{B,obs}})} - 4/3 \tag{A.1}$$

In this relation, y_{O2} is assumed to be an average value. a_i, ρ_c, T_m, D, t_B, R and P_{tot} are initial burning particle radius, initial particle density, film temperature between the char particle and flow, bulk diffusion coefficient of O_2 in the diluents gas, observed particle burnout time, gas universal constant and total pressure of the system, respectively.

If y_{O_2s} is zero or close to zero, the combustion takes place at diffusion limited conditions (Regime III), whereas if y_{O_2s} is close to $y_{O_2\infty}$, the combustion occurs at kinetically limited conditions (Regime I). Any y_{O_2s} in-between the above values results in kinetic-diffusion limited condition (Regime II).

The time t_B required for combustion under diffusion control (Regime III) becomes [32]:

$$t_B = \frac{\rho_c(a_i^2 - a_f^2)}{56}\frac{R T_m}{D}\frac{1}{\ln(1 + \frac{3}{4} y_{O_2\infty})} \tag{A.2}$$

In Eq. A.2, a_f is the final particle radius after extinction, which herein is calculated based on the ash content in the parent coal composition and assuming shrinking core combustion and comparable char and ash residue densities [14].

For instance, for anthracite (AC) burning in air with the observed parameters of this study a_{0i}=56.25(μm), a_f=19 (μm), ρ_c=1 (g/cm^3) [33], T_m=1612 K, P_{tot}=1 (atm), $D_{O_2\text{-}N2}$=3.37 (cm^2/s), $t_{B\text{-}obs}$=294 (ms), R=82 (atm.cm^3/mol.K), oxygen mole fraction on the particle surface from A.1, y_{O_2s}, was calculated to be 0.09 and the diffusion limited

22

burnout time from A.2, t_B, was calculated to be 134 (ms). On the other hand, for anthracite (AC) burning in 21%O_2-79%CO_2, T_m=1550 K, $D_{O2\text{-}CO2}$=2.63(cm^2/s), $t_{B\text{-}obs}$=358 (ms) and the rest of parameters are similar to those of combustion in air. In this case, oxygen mole fraction on the particle surface from A.1, $y_{O_2 s}$, was 0.09 and the diffusion limited burnout time from A.2, t_B, was 165 (ms). Therefore, under the experimental conditions of this study, combustion of anthracite in either air or oxy-fuel condition (21%O_2/79%CO_2) took place in Regime II which is a combination of kinetic and diffusion limited cases.

The resulted observed burnout times and calculated diffusion limited burnout times versus oxygen concentration for anthracite (AC), semi-anthracite (HV) and one of the bituminous coals (SAB) in different oxy-fuel condition is shown in Fig. A.1.

Table 1. Proximate and ultimate analyses of the coals

Coal	AC	HVN	UM	SAB
Origin	Spain	Spain	Mexico	S. Africa
Rank	an	sa	mvb	hvb
Proximate Analysis (wt.%, db)				
Ash	14.2	10.7	21.1	15.0
V.M.	3.6	9.2	23.7	29.9
F.C.[a]	82.2	80.1	55.2	55.1
Ultimate Analysis (wt.%, daf)				
C	94.7	91.7	86.2	81.5
H	1.6	3.5	5.5	5.0
N	1.0	1.9	1.6	2.1
S	0.7	1.6	0.8	0.9
O[a]	2.0	1.3	5.9	10.5
High heating value (MJ kg^{-1}, db)	29.2	31.8	27.8	27.8

an: anthracite; sa: semi-anthracite; mvb: medium-volatile bituminous coal; hvb: high-volatile bituminous coal.
db: dry basis; daf: dry and ash free bases
[a] Calculated by difference.

Table 2. Oxygen content in the O_2/CO_2 required to achieve the same char and volatile temperature as in air-firing conditions.

	AC	HVN	UM	SAB
Equivalent $T_{volatile}$	-	-	35.7	36.2
Equivalent T_{char}	32.8	31.5	29.4	34.1
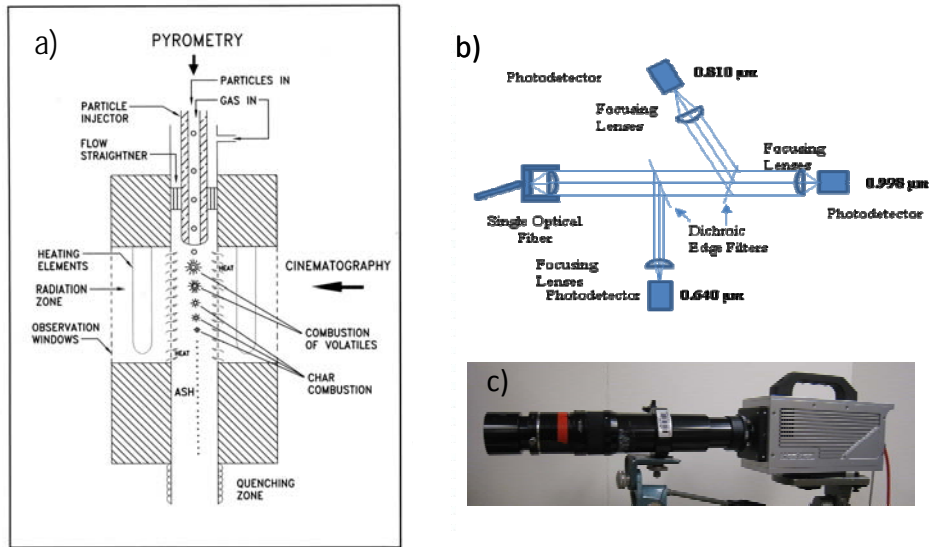
Figure 1. Schematic of the experimental setup and diagnostic facilities. (a) Drop tube furnace (DTF), (b) three-color optical pyrometer and (c) high speed camera.
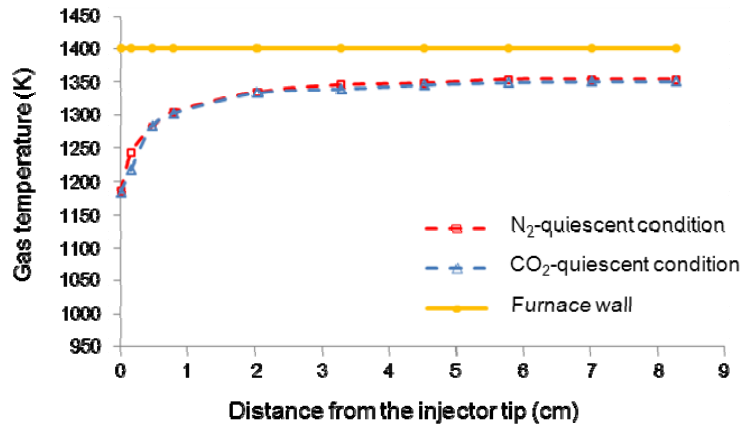
Figure 2. Centerline gas temperature inside the drop-tube furnace filled with either neat N_2 or neat CO_2. The furnace wall temperature was set at 1400 K.
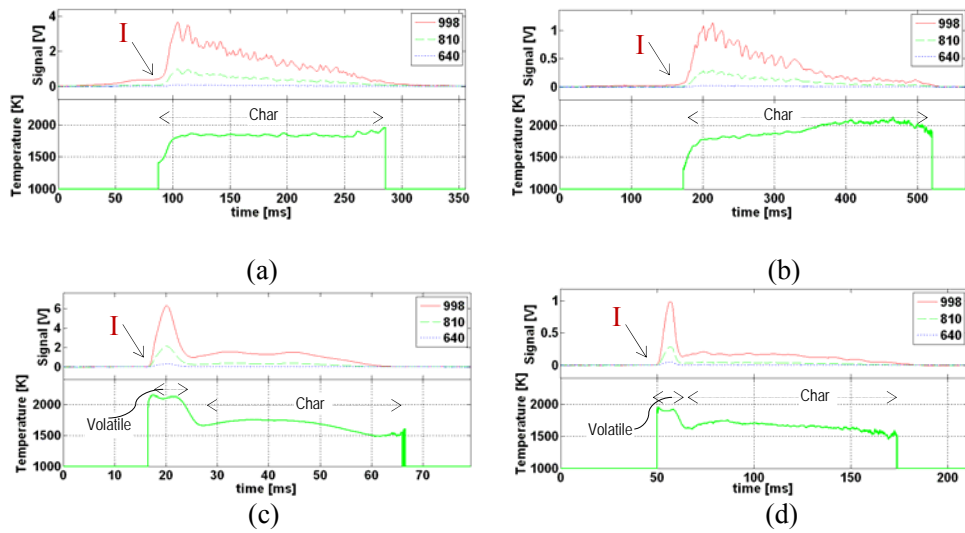
Figure 3. Examples of pyrometric profiles of (a) anthracite (AC), (b) semi-anthracite (HVN), (c) hvb bituminous (SAB), (d) mvb bituminous (UM) particles (75-150 μm) during their combustion in air, at a wall temperature of 1400 K and their deduced particle temperatures. Volatile flame and char combustion phases are denoted. The three pyrometric signals were centered at 998, 810 and 640 nm. I stands for the onset of ignition.

Anthracite (AC) at 21%O_2/79%N_2
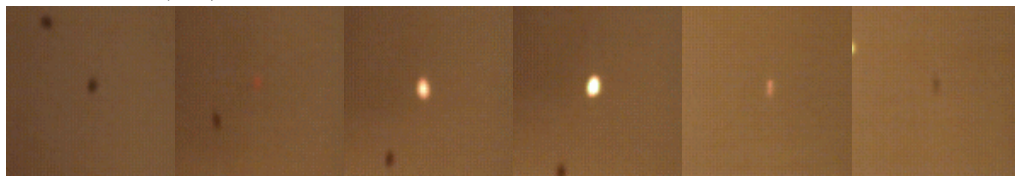
| 0 | 6 | 33 | 36 | 175 | 217 |

Anthracite (AC) at 21%O_2/79%CO_2

| 1 | 8 | 11 | 24 | 63 | 75 |

Anthracite (AC) at 30%O_2/70%CO_2

| 0 | 6 | 10 | 17 | 31 | 38 |

Anthracite (AC) at 50%O_2/50%CO_2

| 1 | 5 | 16 | 40 | 58 | 72 |

Figure 4. High-speed, high magnification cinematography images of single particles (75-150 μm) of anthracite coal (AC) in air and different O_2/CO_2 atmospheres. The displayed numbers in each frame denote milliseconds. A thermocouple wire (100 μm) is shown in the 21%O_2/79%CO_2 case to facilitate assessment of the particle/flame size.
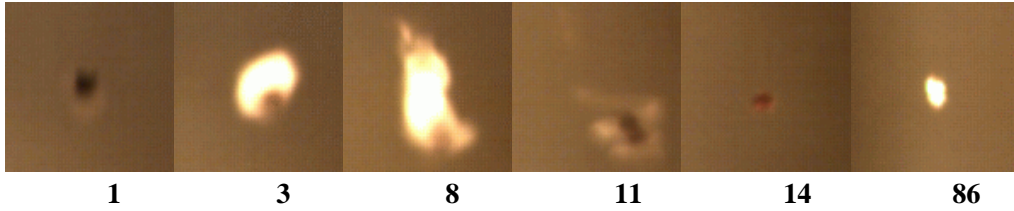
Semi-anthracite (HVN) at 21%O_2/79%N_2
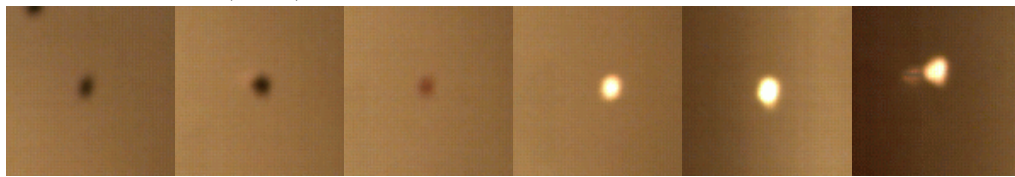
| 0 | 8 | 15 | 19 | 93 | 150 |

Semi-anthracite (HVN) at 21%O_2/79%CO_2

| 1 | 9 | 15 | 47 | 73 | 85 |

Semi-anthracite (HVN) at 30%O_2/70%CO_2
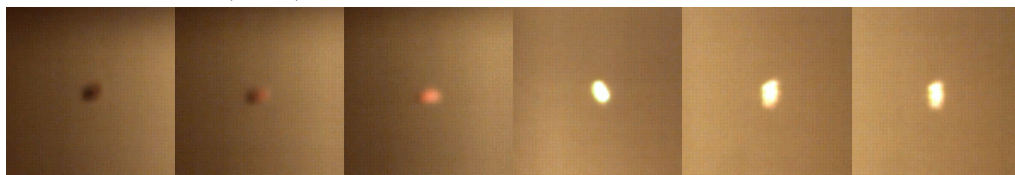
| 1 | 4 | 6 | 62 | 113 | 115 |

Semi-anthracite (HVN) at 50%O_2/50%CO_2

| 0 | 2 | 5 | 8 | 10 | 17 |

Figure 5. High-speed, high magnification cinematography images of single particles (75-150 μm) of semi-anthracite coal (HVN) in air and different O_2/CO_2 atmospheres. The displayed numbers in each frame denote milliseconds.

Bituminous (UM) at 21%O_2/79%N_2

0	1	4	12	15	33
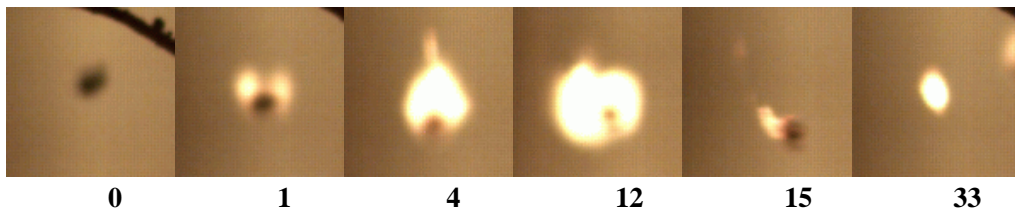
Bituminous (UM) at 21%O_2/79%CO_2

1	3	12	16	19	50
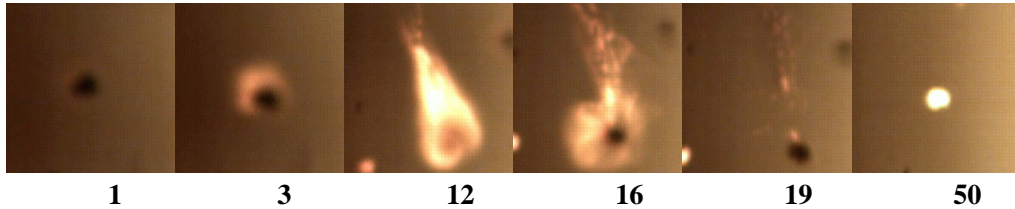
Bituminous (UM) at 30%O_2/70%CO_2

1	2	6	8	11	52
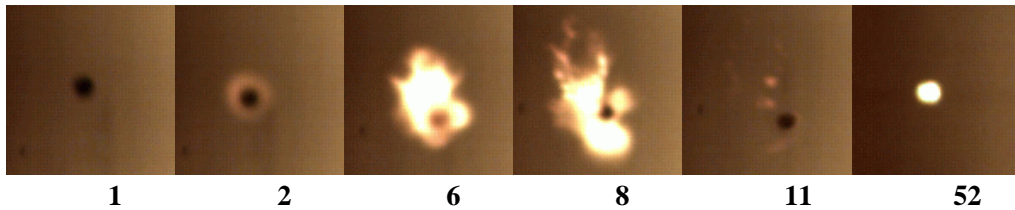
Bituminous (UM) at 50%O_2/50%CO_2

|					
0	1	4	9	13	76
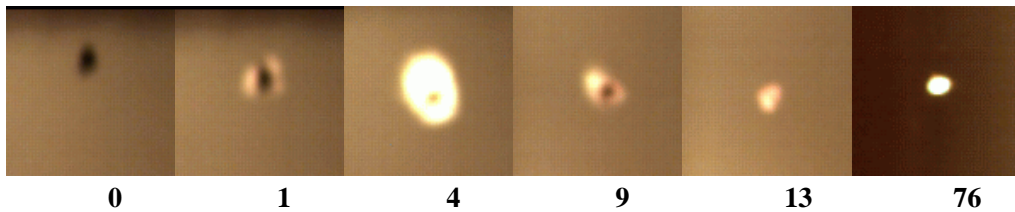
Figure 6. High-speed, high magnification cinematography images of single particles (75-150 μm) of medium volatile bituminous coal (UM) in air and different O_2/CO_2 atmospheres. The displayed numbers in each frame denote milliseconds. A thermocouple wire (100 µm) is shown in the 21%O_2/79%N_2 case to facilitate assessment of the particle/flame size.

Bituminous (SAB) at 21%O$_2$/79%N$_2$

| 0 | 2 | 6 | 23 | 59 | 119 |
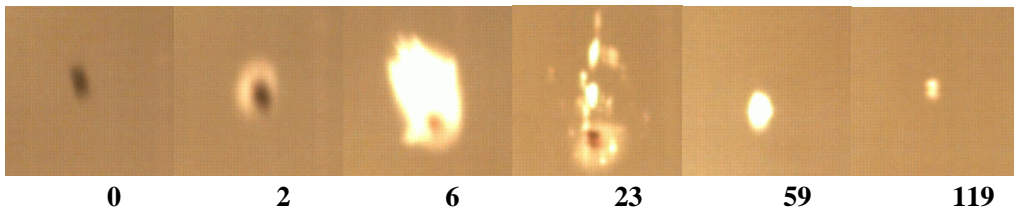
Bituminous (SAB) at 21%O$_2$/79%CO$_2$

| 1 | 6 | 9 | 21 | 29 | 44 |
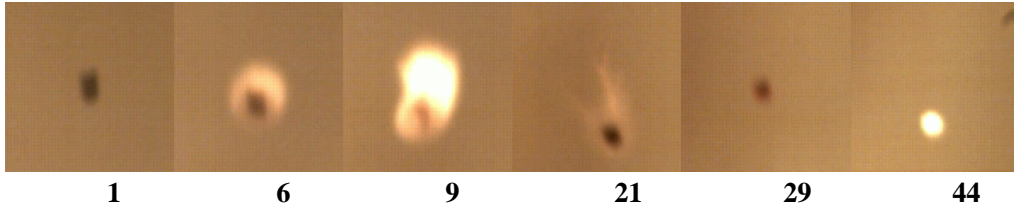
Bituminous (SAB) at 30%O$_2$/70%CO$_2$

| 1 | 3 | 8 | 11 | 14 | 86 |

Bituminous (SAB) at 50%O$_2$/50%CO$_2$

| 0 | 1 | 4 | 10 | 31 | 69 |
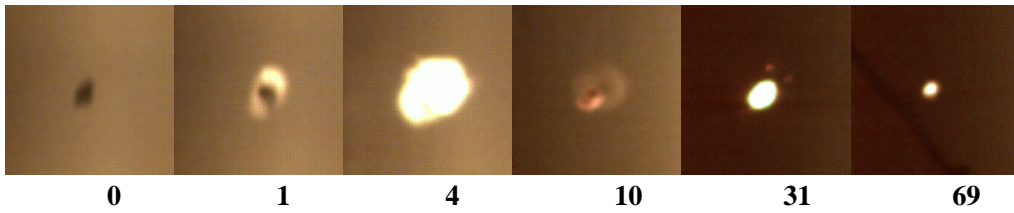
Figure 7. High-speed, high magnification cinematography images of single particles (75-150 μm) of high volatile bituminous coal (SAB) in air and different O$_2$/CO$_2$ atmospheres. The displayed numbers in each frame denote milliseconds.
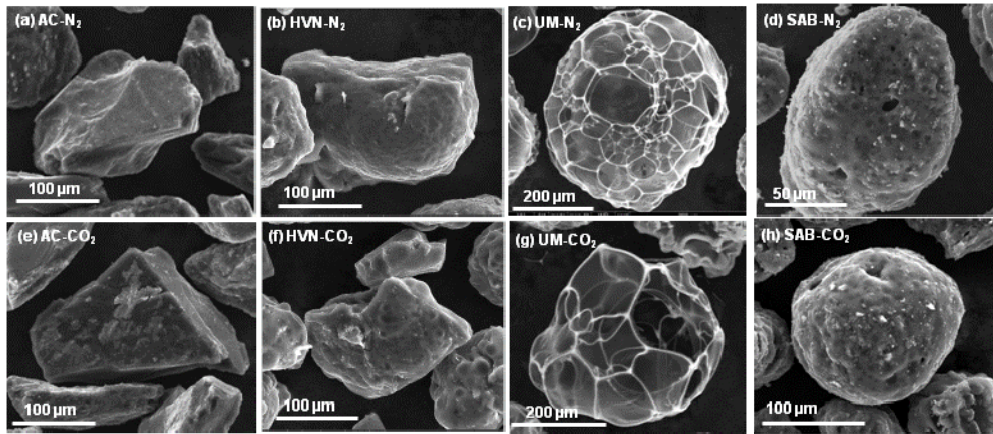
Fig. 8. SEM images of the anthracite (AC), semi-anthracite (HVN) and medium- and high-volatile bituminous (UM, SAB) coal char particles obtained under N_2 (a–d) and CO_2 (e–h) in an entrained flow reactor (EFR) at 1273 K and a particle residence time of 2.5 s [19].

(a)

(b)
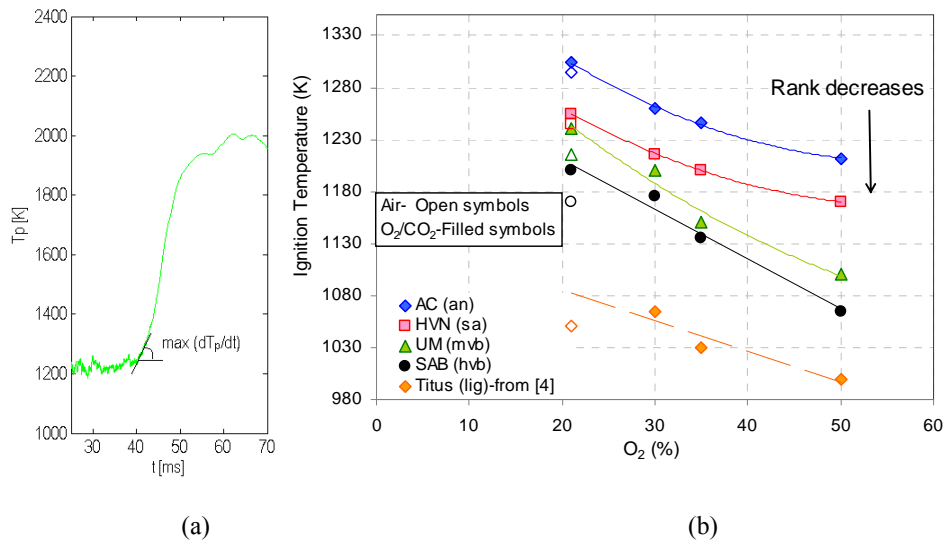
Figure 9. (a) Typical ignition temperature criterion for a pyrometric profile which is defined as the point where the maximum particle temperature gradient was recorded (b) Average deduced ignition temperatures for the four coals of the current study in air and different oxy-fuel environments. Ignition temperatures of lignite, a low rank coal, were also inserted herein from a previous study in this laboratory [4].
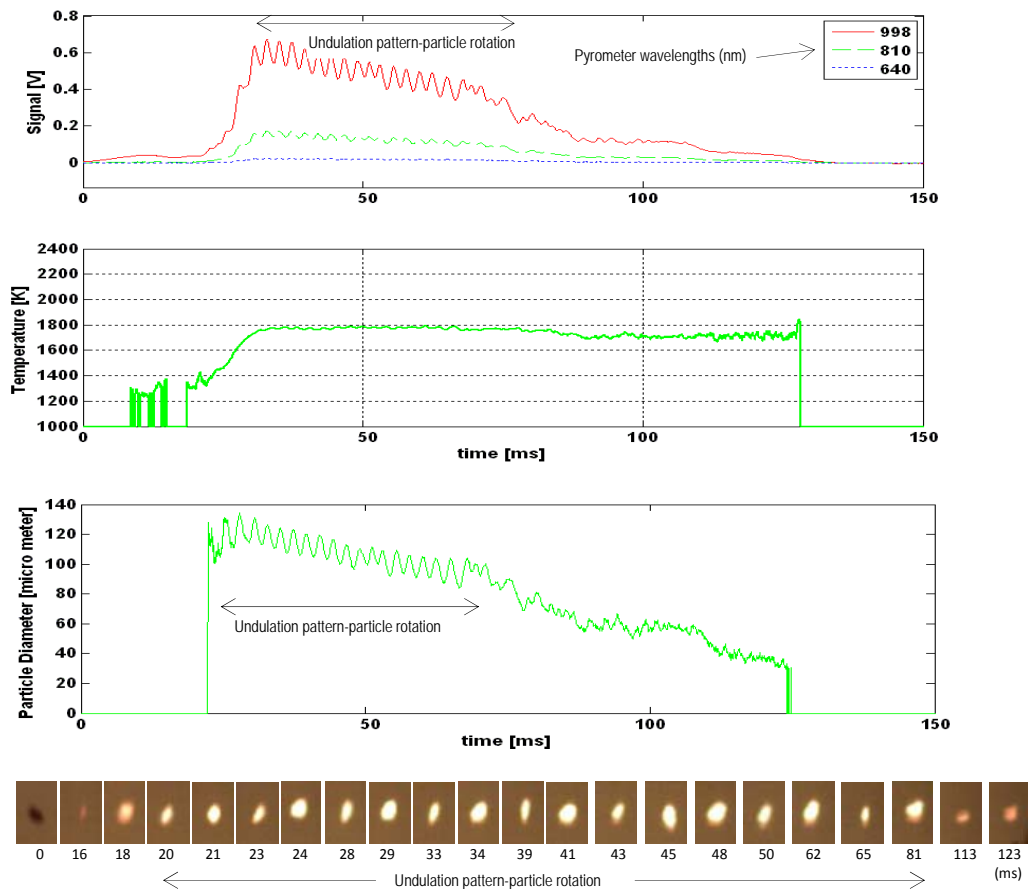
Figure 10. An example of a pyrometric profile of an anthracite coal particle (75-150 μm) burning in air, at a wall temperature of 1400 K and its deduced particle temperature profile.
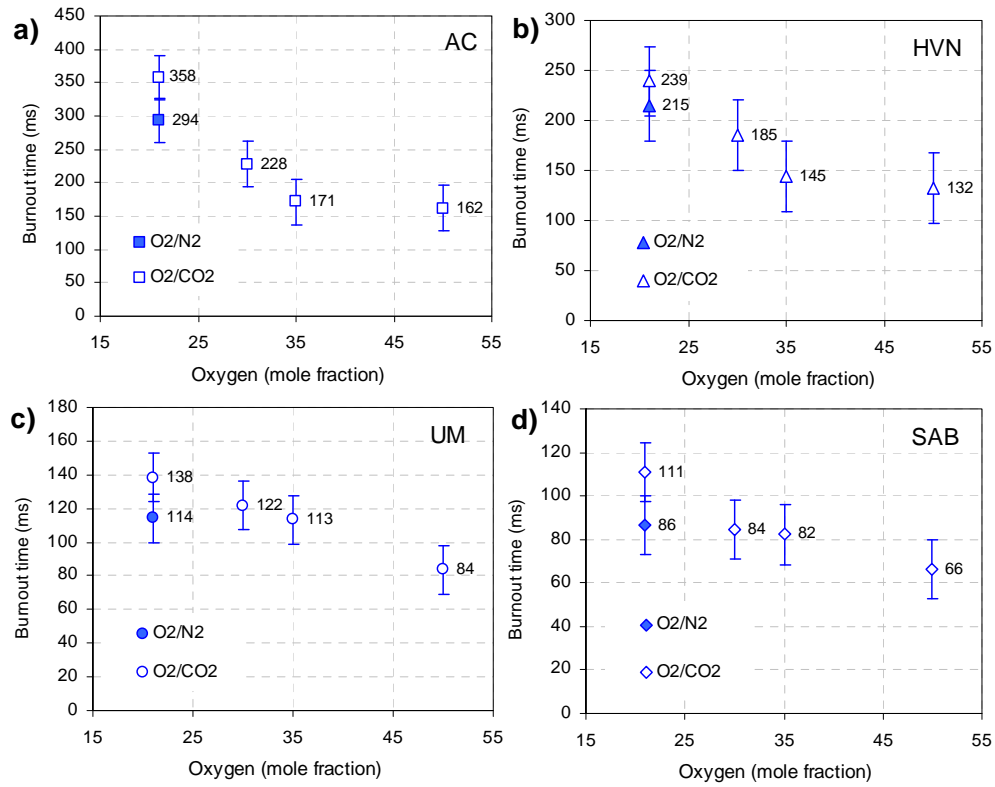
Figure 11. Average burnout times for the four coals (a-d) studied in air and different oxy-fuel environments. The error bars represent standard deviations of the data (2σ).
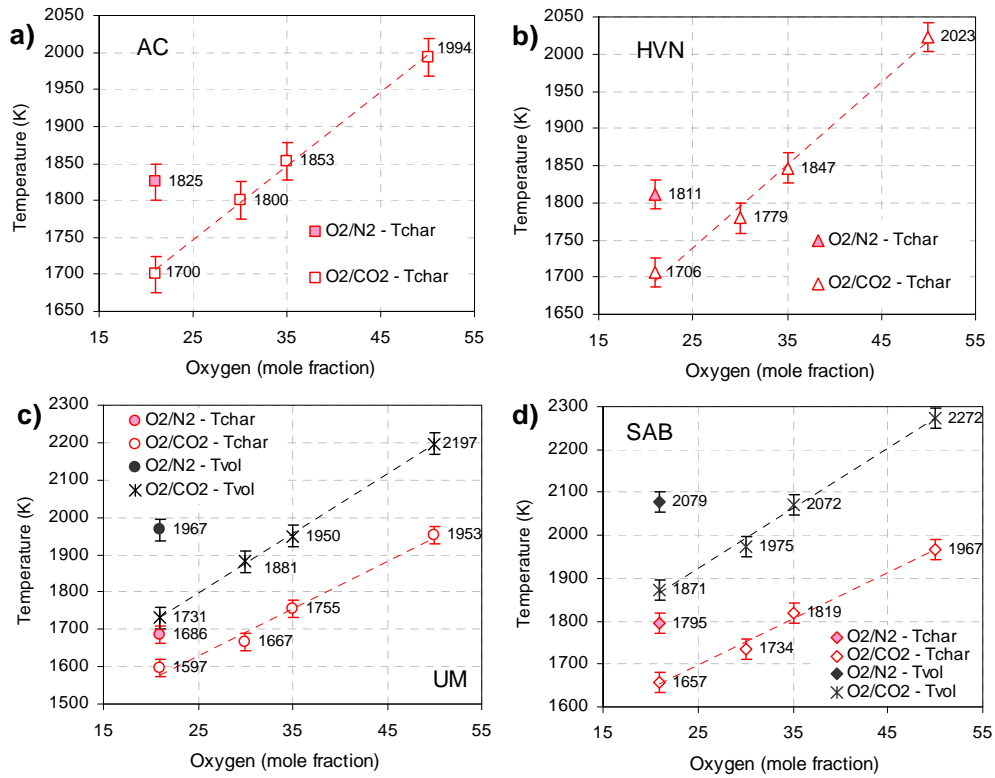
Figure 12. Average char and volatile matter combustion temperatures for the four coals studied (a-d) in air and different oxy-fuel environments. The error bars represent standard deviations of the data (2σ).
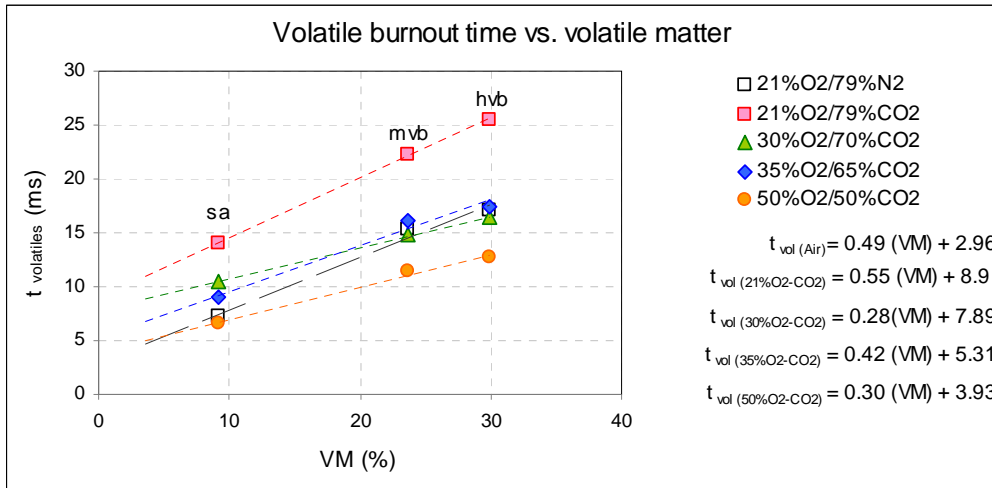
Figure 13. Average observed volatile burnout times versus volatile matter content (VM) of the coals. The experiment was performed at 1400 K furnace temperature with particle diameters in the range 75 µm to 150 µm.
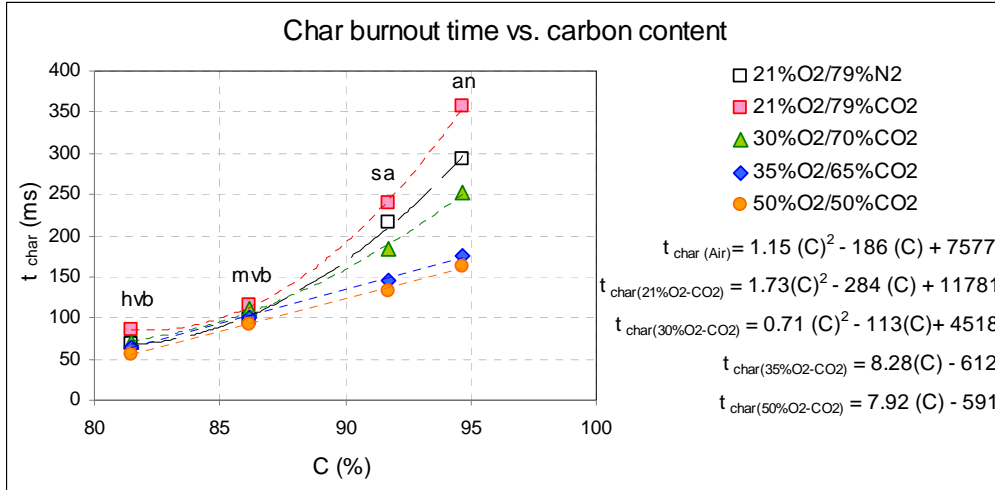
Figure 14. Average char burnout times versus carbon content (C) of the coals. The experiment was performed at 1400 K furnace temperature with particle diameters in the range 75 µm to 150 µm.
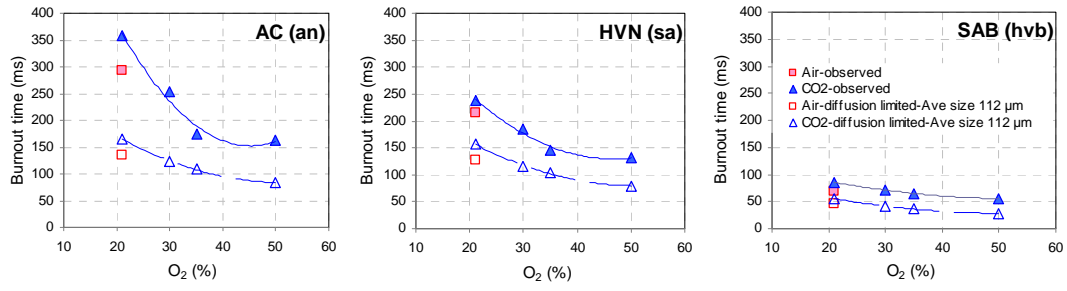
Figure A.1. Comparison of experimentally-observed and calculated diffusion-limited burnout times of anthracite, semi-anthracite and bituminous char particles, plotted against bulk oxygen mole fraction.